Running head: Animal movement and spatio-temporal disease dynamics

Title: A framework for leveraging animal movement to understand spatio-temporal disease dynamics

Authors: Mark Q. Wilber[1,a], Anni Yang[2,3,4,b], Raoul Boughton[5,c], Kezia R. Manlove[6,d], Ryan S. Miller[7,e], Kim M. Pepin[2,f], George Wittemyer[3,g]

Author affiliations:
[1]Forestry, Wildlife, and Fisheries, University of Tennessee, Institute of Agriculture, Knoxville, TN, 37996, mwilber@utk.edu

[2]United States Department of Agriculture, Animal and Plant Health Inspection Service, Wildlife Services, National Wildlife Research Center, Fort Collins, Colorado

[3]Department of Fish, Wildlife and Conservation Biology, Colorado State University, Fort Collins, CO 80523

[4]Department of Geography and Environmental Sustainability, University of Oklahoma, Norman, OK, 73019

[5]Archbold Biological Station, Buck Island Ranch, Lake Placid, FL 33852

[6]Department of Wildland Resources and Ecology Center, Utah State University, Logan, UT, 84322

[7]Center for Epidemiology and Animal Health, United States Department of Agriculture, Animal and Plant Health Inspection Service, Veterinary Service, Fort Collins, CO, 80526

[a]mwilber@utk.edu

[b]anni.yang@ou.edu

[c]raoul.boughton@gmail.com

[d]kezia.manlove@usu.edu

[e]ryan.s.miller@usda.gov

[f]kim.m.pepin@usda.gov

[g]g.wittemyer@colostate.edu

Corresponding author: Mark Q. Wilber, mwilber@utk.edu, Forestry, Wildlife, and Fisheries, 51D McCord Hall, 2640 Morgan Circle Drive, University of Tennessee, Knoxville, TN, 37996, 865-974-8091

Data accessibility statement: The data and code necessary to reproduce our analyses are provided at https://github.com/mqwilber/moveSTIR and will be archived in a public data repository if the manuscript is accepted.

Authorship statement: All authors contributed to the conceptual and mathematical development of the framework. MW and AY ran the analyses. RB collected and provided the data. MW wrote the first draft. All authors contributed substantially to revisions.

Article type: Method

Word count abstract: 150

Word count main text: 4999

Number of figures, tables, or boxes: 5 figures, 1 table

Number of references: 65

Keywords: contact networks; transmission; graph theory; dynamic networks; continuous-time movement models; R_0; individual heterogeneity; direct contact, indirect contact

Abstract

The ongoing explosion of fine-resolution movement data in animal systems provides a unique opportunity to empirically quantify spatial, temporal, and individual variation in transmission risk and improve our ability to forecast disease outbreaks. However, we lack a generalizable framework that can leverage movement data to quantify transmission risk and how it affects pathogen invasion and persistence on heterogeneous landscapes. We developed a flexible framework "Movement-driven modeling of spatio-temporal infection risk" (MoveSTIR) that leverages diverse data on animal movement to derive metrics of direct and indirect contact by decomposing transmission into constituent processes of contact formation and duration and pathogen deposition and acquisition. We use MoveSTIR to demonstrate that ignoring fine-scale animal movements on actual landscapes can mis-characterize transmission risk and epidemiological dynamics. MoveSTIR unifies previous work on epidemiological contact networks and can address applied and theoretical questions at the nexus of movement and disease ecology.

Introduction

Host contact and transmission processes are fundamental drivers of pathogen emergence and spread (McCallum *et al.* 2001; Begon *et al.* 2002; Hopkins *et al.* 2020), but the environmental forces shaping these drivers remain poorly understood. Determining how and why transmission rates vary across the landscape can identify potential transmission hotspots, determine which individuals are involved in their generation, and optimize disease control strategies (Paull *et al.* 2012; Parratt *et al.* 2016). However, obtaining precise, accurate, and spatially explicit transmission metrics remains a major challenge in epidemiology and disease ecology (Albery *et al.* 2020b).

The increasing ubiquity of movement data in livestock and wildlife systems provides a unique opportunity to empirically quantify spatial, temporal, and individual variation in transmission risk (Jacoby & Freeman 2016; Dougherty *et al.* 2018). The data range from high-resolution GPS locations recording animal movements (Hooten *et al.* 2017), proximity loggers, camera traps or acoustic monitors that detect hosts in the vicinity of other hosts or at specific locations (Stehlé *et al.* 2011b; Lavelle *et al.* 2016; Burton *et al.* 2015), and spatially explicit capture-recapture data that provide time-series of host movements between habitat patches or point locations (Cayuela *et al.* 2017; Royle *et al.* 2014; Silk *et al.* 2021). While most of these data sources can and have served as a basis for construction of spatially-explicit contact networks, discrete treatment of observations limits inference on contacts that are in reality occurring in continuous time. Outstanding challenges include scaling detected contacts that are collected at fixed time intervals to those that

occur in continuous time, and rooting emergent networks in epidemiological theory to accurately capture pathogen transmission. While there has been notable recent progress towards inferring contact structure from continuous-time animal movements (Gurarie & Ovaskainen 2013; Noonan *et al.* 2021), these approaches have lacked an epidemiological focus, limiting their ability to describe pathogen transmission.

Movement data provide means to consider components of transmission that are often ignored. While it is standard to decompose transmission into contact and probability of infection given contact (Begon *et al.* 2002), transmission can be decomposed further into constituent sub-processes that better capture observed heterogeneity in transmission risk on actual landscapes (VanderWaal *et al.* 2016; McCallum *et al.* 2017). At a minimum, movement data can capture four processes related to transmission: contact formation (Craft 2015), contact duration (Stehlé *et al.* 2011a; Aiello *et al.* 2016; Springer *et al.* 2017), pathogen deposition potential (Handel & Rohani 2015; Lunn *et al.* 2019), and pathogen acquisition risk (Shahzamal *et al.* 2019). Decomposing transmission into these processes holds value when pathogen life histories are more reliant on one process than another (e.g., contact duration vs. formation), such that a coarse description of contact (e.g., without accounting for variation in contact duration) might misspecify transmission rate. Despite the recent call to better incorporate movement data into disease ecology (Dougherty *et al.* 2018; Manlove *et al.* 2021), we still lack a generalizable, mechanistic framework that can i) leverage the diversity of available movement data to estimate the distinct contribution of each process to aggregate patterns of transmission relevant contact, and ii) determine how inferred patterns of spatial, temporal, and individual-level variability in transmission risk can affect population-level pathogen invasion and persistence on heterogeneous landscapes. A theoretical framework achieving these goals could unify movement and disease ecology, improving our ability to account for realistic sources of variation when predicting transmission risk across landscapes. Such a framework also has the potential to leverage high resolution mobility data in human systems to better forecast outbreak dynamics and effects of interventions (Wesolowski *et al.* 2016; Meekan *et al.* 2017; Miller *et al.* 2019).

Epidemiological network models provide the foundations for representing variation in contact and transmission (Bansal *et al.* 2007; White *et al.* 2017; Silk *et al.* 2017, 2019). However, many network models used in epidemiology are temporally static and account only for contact formation, while overlooking variable contact duration and pathogen deposition and acquisition processes (Craft 2015; VanderWaal *et al.* 2016; Enright & Kao 2018). Static networks can also fail to accurately predict disease dynamics on networks when the presence of nodes (e.g., the presence of individuals in a population) and edges (e.g., links between two individuals) change through time or differ in type (Fefferman & Ng 2007; Springer *et al.* 2017). Dynamic epidemiological network models ameliorate some of these limitations by allowing for individual-level variation in contact duration and intensity as the nodes and edges vary through time (Holme & Saramäki 2012; Holme

& Liljeros 2014; Richardson & Gorochowski 2015). But even dynamic network models have important limitations. First, they still rarely account for spatial heterogeneity in contact and transmission (Manlove *et al.* 2018; Albery *et al.* 2020a) and its landscape drivers, limiting their application in traditional models of spatial transmission. Second, inferences of network structure are often phenomenological rather than based on the dynamic processes that structure the network, which limits prediction of contact and transmission processes across demographic and environmental conditions. Third, in both aspatial and network-based host-pathogen models, direct and indirect transmission often are modeled as two distinct processes (Springer *et al.* 2017; Silk *et al.* 2018; Wilber *et al.* 2019; Yang *et al.* 2020), failing to recognize the continuum spanning direct to indirect contacts (i.e., transmission potential of short to long term direct contact may overlap with short to long term indirect contact) (Richardson & Gorochowski 2015; Shahzamal *et al.* 2019). Finally, "edges" in indirect contact networks are often quantified using metrics such as home-range overlap (Godfrey *et al.* 2010; Springer *et al.* 2017), which ignore potentially important fine-scale spatial variation in host space use (Albery *et al.* 2020a).

Here, we develop and apply a novel framework that we refer to as "Movement-driven modeling of spatio-temporal infection risk" (MoveSTIR), which can leverage diverse and widely available spatial and temporal data on animal movement and proximity (via GPS tracking, camera grids, proximity collars, spatially explicit capture-recapture or acoustic monitors) to derive heterogeneous metrics of contact and, ultimately, make empirically-informed predictions of disease risk on real landscapes (Figure 1). MoveSTIR captures contact heterogeneity in terms of type and strength along the continuum of indirect and direct contacts, while simultaneously accounting for other constituent components of transmission, such as contact duration, pathogen acquisition, pathogen deposition, and pathogen decay. Importantly, by leveraging the extensive and growing archive of movement-related data on thousands of taxa currently available in databases such as MoveBank (5,915 studies across 1,025 taxa and billions of data points as of 2021; Kranstauber *et al.* 2011), MoveSTIR is broadly applicable without necessarily needing simultaneous infection data. While pairing MoveSTIR with epidemiological data will further increase its realm of inference, a strength of MoveSTIR is that it generalizes and extends many previous approaches for deriving and analyzing observed contact networks (e.g., Richardson & Gorochowski 2015; Springer *et al.* 2017; Enright & Kao 2018; Silk *et al.* 2018; Wilber *et al.* 2019), providing a common foundation for empirically driven, prospective analyses of spatio-temporal disease risk. We show how MoveSTIR can benefit inference of disease dynamics in wildlife, livestock, and human systems and demonstrate with a real example how failing to account for fine-scale individual movements can significantly mis-represent potential epidemiological dynamics.

Material and methods

Building MoveSTIR from epidemiological theory

MoveSTIR begins from a simple compartmental host-parasite model that tracks **S**usceptible and **I**nfected host density and the density of the **P**athogen in the environment. We make the following assumptions: i) the force of infection (FOI) experienced by a susceptible host is a linear function of pathogen density in the environment βP, where β is the transmission rate that combines rates of acquisition and contact, ii) infected hosts deposit pathogen at rate λ, iii) the pathogen decays in the environment at rate ν, iv) the pathogen is well-mixed in the area where contact and acquisition occurs, and v) the infection process does not substantially deplete the pathogen in the environment (Dwyer *et al.* 1997; Fenton *et al.* 2015). These assumptions provide a reasonable starting point for MoveSTIR but can be readily adjusted to account for non-linear FOI or extended to account for states such as **E**xposed and **R**ecovered. For simplicity, we also assume that **I**nfected hosts recover at rate γ and are immediately **S**usceptible. This assumption has no bearing on the derivations in this section.

The following differential equations describe the infection dynamics in a host population

$$\begin{aligned} \frac{dS}{dt} &= -\beta PS + \gamma I \\ \frac{dI}{dt} &= \beta PS - \gamma I \\ \frac{dP}{dt} &= \lambda I - \nu P \end{aligned} \tag{1}$$

where we initially assume a constant population size of $S + I = N$ and no births or deaths.

We can equivalently express equation 1 as a renewal equation (Arino & van den Driessche 2006), namely

$$\begin{aligned} \frac{dS(t)}{dt} &= -\beta P(t)S(t) + \gamma I(t) \\ \frac{dI(t)}{dt} &= \beta P(t)S(t) - \gamma I(t) \\ P(t) &= P_0(t) + \int_0^t \lambda I(u) e^{-\nu(t-u)} du \end{aligned} \tag{2}$$

In equation 2, $I(u)$ gives the density of infected individuals at some previous time u, $u < t$. The function $e^{-\nu(t-u)}$ defines the pathogen survival function in the environment, assuming that the pathogen decays at a constant rate ν. We could readily replace $e^{-\nu(t-u)}$ with any survival function reflective of the pathogen of interest. The parameter $P_0(t)$ is the density of pathogen present at time 0 that are still present at time t.

We can then substitute in the expression of $P(t)$ to re-write $\frac{dI(t)}{dt}$ as a function of $I(u)$

$$\frac{dI(t)}{dt} = S(t)\beta \int_0^t \lambda I(u) e^{-\nu(t-u)} du - \gamma I(t) \tag{3}$$

where we assume $P_0(t) = 0$.

The function $h(t) = \beta \int_0^t \lambda I(u) e^{-\nu(t-u)} du$ is the per capita FOI at time t. The FOI $h(t)$ is a rate with units time^{-1}. As such, $h(t)$ defines the FOI felt by an individual at a given moment after accounting for the time-dependent accumulation and decay of all pathogens previously deposited by infected hosts. Importantly for the development of our framework, $h(t)$ lets deposition rate (λ) and contact formation and acquisition of the pathogen (both encapsulated in β) vary independently, and allows for a continuum between direct contact (when $u \approx t$) and indirect contact (when $u < t$). However, equation 3 does not i) clearly separate contact formation and pathogen acquisition, ii) explicitly account for contact duration, or iii) account for directional differences in transmission risk due to the order of when individuals visit locations. For this, we extended equation 3 to consider directional interactions occurring at the individual level.

A pairwise view of the force of infection (FOI)

Consider a single individual i moving through space. At each moment, the individual experiences a FOI dependent upon the full history of infected individuals that previously or presently share its current location. Let $I(u, x)$ be the number of infected hosts in location x at time u. If there are $N - 1$ other hosts in the population, we can write $I(u, x) = \sum_{j=1}^{N-1} \delta_{x_j(u)}(x) \delta_{I_j(u)}(I)$. The function $\delta_{x_j(u)}(x)$ is an indicator function that is defined as

$$\delta_{x_j(u)}(x) = \begin{cases} 1 & \text{if the location of host } j \text{ at time } u \text{ is } x \text{ (i.e., } x_j(u) = x) \\ 0 & \text{otherwise} \end{cases}$$

Similarly, $\delta_{I_j(u)}(I)$ is the indicator function

$$\delta_{I_j(u)}(I) = \begin{cases} 1 & \text{if host } j \text{ is infected at time } u \text{ (i.e., } I_j(u) = I) \\ 0 & \text{otherwise} \end{cases}$$

Taken together, this means that host j at past time u only gets "counted" toward the FOI experienced by focal host i at time t if they are infected and shedding pathogen ($I_j(u) = I$) at time u and in the same location x ($x_j(u) = x$).

With this individual-level view, we can update $h(t)$ to consider the contributions from other individual hosts to the FOI felt by a focal host i at time t in location x.

$$
\begin{aligned}
h_i(t,x) &= \beta' \int_0^t \sum_{j=1}^{N-1} \lambda \delta_{x_j(u)}(x) \delta_{I_j(u)}(I) e^{-\nu(t-u)} du \\
&= \underbrace{\sum_{j=1}^{N-1}}_{\text{Sum over individuals}} \int_0^t \underbrace{\beta'}_{\text{Acquisition}} \underbrace{\delta_{x_j(u)}(x)}_{\text{Contact}} \underbrace{\lambda \delta_{I_j(u)}(I)}_{\text{Deposition}} \underbrace{e^{-\nu(t-u)}}_{\text{Pathogen decay}} du
\end{aligned} \tag{4}
$$

where β' is now an acquisition rate (i.e., an uptake rate times per pathogen probability of infection) as we have conditioned on contact with the term $\delta_{x_j(u)}(x)$. Consider a single term in the summation, $h_{i \leftarrow j}(t,x) = \int_0^t \beta' \delta_{x_j(u)}(x) \lambda \delta_{I_j(u)}(I) e^{-\nu(t-u)} du$. We can define this term as: the FOI felt by individual $i \neq j$ at time t in location x due to individual j's previous infection history in location x, up to time t. This quantity is a rate with units time^{-1} and encapsulates pathogen acquisition, contact formation, pathogen deposition, and direct and indirect transmission. Note because pairwise FOI is asymmetrical $h_{i \leftarrow j}(t,x)$ does not necessarily equal $h_{j \leftarrow i}(t,x)$. Moreover, contact duration is explicitly accounted for by the integral over $\delta_{x_j(u)}(x)$, which specifies how long host i is in contact with host j in the past (indirect) or present (direct). Finally, we can more explicitly account for the area of location x by re-writing $\beta' \delta_{x_j(u)}(x)$ as $\tilde{\beta} \Phi(x_j(u), x)$ (Gurarie & Ovaskainen 2013; Martinez-Garcia *et al.* 2020), where $\tilde{\beta}$ has units $\frac{\text{area units}}{\text{time}}$ (e.g., $\frac{m^2}{\text{hour}}$). The function $\Phi(x_j(u), x)$ is the contact function and is a probability density function that integrates to one over the spatial domain of interest with units 1/area units (e.g., see Appendix S1.1; Gurarie & Ovaskainen 2013).

Quantifying FOI from movement data: the transmission kernel

How do movement data inform the FOI that individual j imposes on individual i at time t in location x, $h_{i \leftarrow j}(t,x)$? Here, we focus our discussion and examples on high-resolution GPS tracking data that are commonly collected in human, livestock, and wildlife systems. However, MoveSTIR is broadly applicable to many types of movement, proximity, and co-occurrence data that are widely available across thousands of animal taxa (Appendix S2; Kranstauber *et al.* 2011).

Let $\mathbf{s}(t)$ be a continuous-time movement trajectory that gives the spatial location of an individual at any time t. While we typically do not know $\mathbf{s}(t)$, recent developments in movement ecology provide statistical tools to estimate $\mathbf{s}(t)$ from GPS tracking data (Johnson *et al.* 2008; Calabrese *et al.* 2016; Hooten *et al.* 2018). This highlights a key advantage of MoveSTIR – it builds directly from state-of-the-art continuous-time movement models to improve inference on spatio-temporal infection risk. Here, we assume that $\mathbf{s}(t)$ has already been estimated. Moving forward, we use the simpler notation $h_{i \leftarrow j}(t)$ to specify the FOI, recognizing that if we have an estimate of the movement trajectory $\mathbf{s}(t)$, time t already implies location x.

To capture FOI exerted along entire movement trajectories, we must aggregate the spatially explicit force

defined by $h_{i \leftarrow j}(t)$ to all of the various locations visited by both individuals from the focal pair. Consider two hosts moving through space and time with movement trajectories $\mathbf{s}_1(t)$ and $\mathbf{s}_2(t)$. We define a transmission kernel $K_{a_2 \leftarrow d_1}(\tau_a, \tau_d)$ that specifies the transmission weight resulting from host 2 at time τ_a contacting past host 1 at time τ_d (and vice versa). The "a" identifies τ_a as the time for the host acquiring pathogen and the "d" identifies τ_d as the time for the host depositing pathogen. Similarly, the notation $a_2 \leftarrow d_1$ indicates that host 2 is the host acquiring pathogen by encountering the past pathogen deposited by host 1. Mathematically, $K_{a_2 \leftarrow d_1}(\tau_a, \tau_d)$ defines the spatio-temporal acceleration in FOI and has units time^{-2}.

The transmission kernels $K_{a_i \leftarrow d_j}(\tau_a, \tau_d)$ are the core of MoveSTIR (Fig. 1). Based on our motivating example given in equation 4, we can define $K_{a_i \leftarrow d_j}(\tau_a, \tau_d)$ as

$$K_{a_i \leftarrow d_j}(\tau_a, \tau_d) = \begin{cases} \underbrace{[\tilde{\beta}]}_{\text{Acquisition}} \underbrace{[\Phi(\mathbf{s}_j(\tau_d), \mathbf{s}_i(\tau_a))]}_{\text{Contact}} \underbrace{[\lambda \delta_{I_j(\tau_d)}(I)]}_{\text{Deposition}} \underbrace{[e^{-\nu(\tau_a - \tau_d)}]}_{\text{Pathogen decay}} & \text{for } \tau_d \leq \tau_a \\ 0 & \text{otherwise} \end{cases} \tag{5}$$

where the terms are the same as the integrand in equation 4, with $\beta' \delta_{x_{j(u)}}(x)$ generalized to $\tilde{\beta} \Phi(\mathbf{s}_j(\tau_d), \mathbf{s}_i(\tau_a))$. The condition $\tau_d \leq \tau_a$ indicates that host i (who is acquiring pathogen) can contact the current and past trajectory of host j (who is depositing pathogen), but not its future trajectory. The transmission kernel $K_{a_i \leftarrow d_j}(\tau_a, \tau_d)$ is not restricted to the form shown in equation 5 and can be modified according to the biology of the focal host-parasite system (see Appendix S1.2).

Understanding the transmission kernel $K_{a_i \leftarrow d_j}(\tau_a, \tau_d)$

Once parameterized from movement data, the transmission kernel $K_{a_i \leftarrow d_j}(\tau_a, \tau_d)$ can be integrated over different dimensions to provide windows into how individual-level infection risk experienced by a host varies in space and time (Table 1; toy examples in Appendix S1.3). There are, however, two distinct ways to explore the transmission kernel $K_{a_i \leftarrow d_j}(\tau_a, \tau_d)$.

First, we can calculate what we will refer to as the *maximum potential infection risk*. For this metric, we assume $\delta_{I_j(\tau_d)}(I)$ is always equal to one (i.e., all hosts are always infected) and ask, what is the maximum possible exposure that a susceptible focal host could experience given the observed movement trajectories of other infected hosts? This is a generalization of the observed "contact network" (*sensu* Craft 2015), but it accounts for the direct to indirect contact continuum.

Second, we are also interested in understanding the "transmission network" (*sensu* Craft 2015) – what we will here describe as *realized infection risk*. Realized infection risk is necessarily less than or equal to the maximum potential infection risk. While difficult to measure empirically, we can derive a model estimate

of the realized infection risk by re-incorporating our transmission kernel into an individual-level model of host-pathogen dynamics. We describe such a model in the section *From the transmission kernel to infection dynamics*. We proceed with maximum potential infection risk, but all the calculations we describe can be done using realized infection risk.

A simulated example

We use the functions in Table 1 to illustrate the descriptive power of the transmission kernel with a simulated example of two hosts moving in continuous time and space (Fig. 2A). These are representative of trajectories from GPS tracking data fit with continuous-time movement models. This example illustrates how MoveSTIR uses movement data to estimate when and where potential infection risk is highest, who is contributing the most to infection risk, and how much maximum potential infection risk is due to direct or indirect transmission (Fig. 2). Code is provided at https://github.com/mqwilber/moveSTIR.

First, we can use the transmission kernel to identify how the maximum potential FOI $h_{1\leftarrow 2}(t)$ and $h_{2\leftarrow 1}(t)$ varies in space and time (Fig. 2). We see that the FOI and cumulative FOI experienced by host 1 and host 2 are highly asymmetric. Because host 1 tends to lead host 2 in space and time, host 1 experiences little FOI from host 2 over the time period when these hosts are tracked *in silico* (Fig. 2B,E). In contrast, host 2 tends to follow host 1 in space and time and experiences moments of elevated FOI as they encounter regions of space where host 1 has previously spent time and potentially deposited pathogen (Fig. 2C,F).

Second, the transmission kernel shows that the relative contributions of direct and indirect transmission to cumulative FOI are distinctly different between the two hosts (Table 1; Fig. 2D). The maximum potential infection risk experienced by host 1 from host 2 is largely due to "direct transmission", i.e., host 1's infection risk is primarily a result of instances when the two hosts were in the same place at nearly the same time. In contrast, "indirect transmission" (here defined as infection risk after a time lag of 0.15 units, Fig. 2D) was responsible for 30% of host 2's potential cumulative FOI, compared a 0% contribution of indirect transmission to host 1's potential cumulative FOI (Fig. 2D).

From the transmission kernel to dynamic networks

MoveSTIR outputs can be represented as a dynamic, epidemiological network (Holme & Saramäki 2012; Enright & Kao 2018). The transmission kernels of MoveSTIR at any given time point t specify a weighted, asymmetrical adjacency matrix, where the weights are the FOI felt by host i from host j at time t ($h_{i\leftarrow j}(t)$, Table 1). Thus, any of the metrics that can be calculated on a dynamic network and are predictive of disease spread (e.g., latency, temporal closeness centrality, burstiness, etc.; Holme & Saramäki 2012) can also be explored within the MoveSTIR framework. Moreover, because a dynamic network can always be

summarized as a static network (with loss of temporal information), insights from MoveSTIR are directly comparable to the vast epidemiological literature that uses static contact networks to make inference on disease dynamics (Silk *et al.* 2017; White *et al.* 2017). This provides exciting opportunities to compare the epidemiological implications of static, weighted networks to dynamic, weighted networks (Stehlé *et al.* 2011a; Springer *et al.* 2017) and build multi-layered networks to understand transmission among species through shared environmental resources (Silk *et al.* 2018; Wilber *et al.* 2019, Appendix S2), all within the MoveSTIR framework. In Appendix S3, we illustrate how MoveSTIR encompasses earlier approaches that use static and dynamic networks.

From the transmission kernel to prospective infection dynamics

MoveSTIR's epidemiological foundation allows it to move directly from spatio-temporally explicit descriptions of host movements across real landscapes (Fig. 2A), to infection risk (Fig. 2B-F), to prospective predictions of disease dynamics in space and time. Thus, MoveSTIR can ask "what if" questions regarding potential interventions aimed at reducing pathogen invasion or persistence.

To address prospective questions with MoveSTIR, we first link the transmission kernels $K_{a_i \leftarrow d_j}(\tau_a, \tau_d)$ directly to an individual-level, continuous-time Markov process that tracks discrete epidemiological states of individuals (e.g., **S**usceptible, **E**xposed, **I**nfected, **R**ecovered, etc.; Appendix S4). After this model is specified, we can directly simulate disease dynamics on the contact network defined by the movement data and encoded in the transmission kernel. Beyond just simulation, we can also use the model to calculate fundamental epidemiological metrics such as R_0 that determines the ability of the pathogen to invade and persist in the population, given the dynamic contact network along a direct to indirect continuum defined by the movement data (Appendix S4; Diekmann *et al.* 2013; Valdano *et al.* 2015; Leitch *et al.* 2019). This allows for extensive sensitivity analysis (without explicit simulation) to test how spatial, temporal, and individual characteristics affect the dynamics of pathogen invasion. In Appendix S4.4, we explore a simulated example to demonstrate how MoveSTIR can combine the transmission kernel and dynamic epidemiological models to ask prospective questions regarding the role of individual, spatial, and temporal processes on pathogen invasion dynamics.

Empirical application of MoveSTIR

We demonstrate the utility of MoveSTIR by investigating the implications of observed wild pig (*Sus scrofa*) movement dynamics on the transmission dynamics of a hypothetical introduction of a pathogen with similar

characteristics to African swine fever virus (ASFV). We asked three questions: i) How much heterogeneity in individual-level infection risk exists in space and time and does ignoring this heterogeneity affect potential epidemiological dynamics? ii) What are the proportional contributions of direct and indirect contact to potential pathogen invasion and iii) What is the spatial scale of potential transmission hotspots on the landscape?

We captured and deployed GPS collars (Catlog GPS device and Lotek LMRT3 VHF Collars, Lotek, WA, US) on 19 adult, free-ranging wild pigs (14 females and 5 males) on a cattle ranch in south Florida from April to August, 2017 (University of Florida IACUC protocol #201408495 and #201808495). The GPS collars were programmed to record a fix every 30 min. We converted the high-resolution movement data to continuous-time movement trajectories discretized to five minute intervals using the R package `ctmm` (Fig. 3, Appendix S5; Calabrese *et al.* 2016).

We assumed that the contact function $\Phi(\mathbf{s}_j(\tau_d), \mathbf{s}_i(\tau_a))$ followed a so-called top-hat function such that contact could only occur when wild pigs were within 10 m of past or present depositing pigs (Appendix S1.1). We chose this threshold as the errors of GPS locations in the study site ranged from 6.6 m in open areas to 8.6 m in closed canopy.

For viral decay in the environment, we used the survival function of an exponential distribution with viral decay rate $\nu = 1/5$ day^{-1}. This is consistent with experiments showing that ASFV can remain infectious in the environment and excreted material from 1 to 30 days depending on environmental conditions (Mazur-Panasiuk *et al.* 2019). Spatio-temporal factors that affect pathogen decay rate can be included within MoveSTIR (Appendix S1.2). Furthermore, we assumed that deposition rate λ and acquisition rate $\tilde{\beta}$ did not depend on host movements or the local environment, though this assumption can be relaxed within MoveSTIR (Appendix S1.2). Because our goal was to make inference on relative infection risk, we did not need to specify exact values for deposition rate λ or acquisition rate $\tilde{\beta}$ as they are constant multipliers (e.g., equation 5) and cancel out when calculating relative infection risk.

We defined direct contact between two hosts as any contact that occurred within a temporal separation of 0 to 5 minutes. We defined indirect contacts as any contact that occurred with a temporal separation of greater than 5 minutes. Of course, MoveSTIR allows us to be flexible with this definition of direct and indirect contact.

Results

Over the four months of the study, MoveSTIR identified that individuals experienced drastically different total potential cumulative FOI (Fig. 4A) and temporal patterns in how FOI accumulated (Fig. 4A). For

example, while individuals 11 and 14 experienced a relatively consistent increase in cumulative FOI over four months, individuals 5, 7 and 19 showed a notable burst of accumulation in FOI over a period from late May to early June. While Fig. 4A illustrates how FOI changes on weekly to monthly time scales, MoveSTIR also allows us to examine how FOI changes over hourly and daily scales (Fig. 4B). For 10 out of the 19 individuals, there was a significant signal of daily periodicity in temporal FOI, meaning that associations that caused peaks in FOI tended to change on a daily temporal scale (Fig. 4B, C).

We used MoveSTIR to derive static, weighted direct and indirect contact networks from the dynamic, weighted networks defined by the transmission kernel (Fig. 5). The edges in these static networks were the (asymmetric) average potential FOI experienced by pairwise interactions between two individuals (see Table 1, Appendix S3). Direct contact networks were drastically less connected (lower mean degree and lower transitivity) than the networks that included both direct and indirect connections (Fig. 5). To examine the consequences of these differences on the relative potential of ASFV invasion into the system, we assumed an Susceptible-Infected-Recovered model for ASFV transmission (Appendix S5). We then computed relative R_0 from a network with only direct transmission, only indirect transmission, and one with both. The relative R_0 values for the indirect network and the network that included both were over 200 times greater than the relative R_0 for a network with only direct contact. While indirect transmission added 126 edges compared to direct contact alone (Fig. 5), the relative increase in R_0 was almost completely related to the increase in average FOI on edges that were already present for direct contacts. While this large effect likely represents an upper bound on the influence of indirect transmission in this system, our results clearly illustrate the sizable importance of indirect transmission for pathogens with even relatively short persistence in the environment (Yang *et al.* 2021).

We used our movement-derived networks to further examine the relative contributions of particular individuals to ASFV invasion potential. Consistent with our analysis on individual heterogeneity in FOI (Fig. 4), removing hosts that experienced high cumulative FOI led to substantially larger proportional reductions in R_0 (between 35%-46%) than removing other individuals (almost always less than 1%) (Fig. 5). To discern epidemiologically relevant behaviors, we calculated the betweenness centrality of individuals in the full static network, a network metric that describes how often an individual lies on the shortest path between two other nodes. We found that individuals with small contributions to R_0 can still have substantial effects on network connectivity and thus pathogen spread in space. Individual 22 had a small relative contribution to R_0 compared to individuals 11, 14, and 17, but was centrally located, bridging highly connected groups of individuals (Fig. 3) and leading to higher betweenness centrality than the other individuals. This result reinforces the limitations of R_0-like metrics for understanding the spatial spread of pathogens in populations (Cross *et al.* 2007).

We compared MoveSTIR predictions of transmission relevant contact networks to previous approaches that used coarser spatial metrics, such as home range overlap, to derive empirically-informed contact networks (e.g., Godfrey *et al.* 2010; Springer *et al.* 2017, Fig. 5, details in Appendix S6). Home range overlap analyses are a special case of MoveSTIR (Appendix S6). We found that home range overlap analysis predicted a similar static, unweighted network structure as MoveSTIR applied to continuous-time, continuous-space movement trajectories (Fig. 5B-C). However, home range overlap missed significant individual-level heterogeneity in the edge weights of the network (Fig. 5B-C), resulting in an R_0 estimate that was 30 times lower than the MoveSTIR estimate and a mis-specification of individual-level contributions to pathogen invasion. This result was consistent across different metrics of home range overlap (Fig. S7). Thus, ignoring fine-scale individual-level heterogeneity in movements within home ranges significantly underestimated predictions of pathogen invasion risk.

Finally, we used MoveSTIR to explore the spatial variation in infection risk on the landscape to identify hotspots of average FOI (Fig. 3). We divided the landscape into grid cells that were approximately 15 by 15 meters and, for each grid cell, calculated the average FOI experienced by individuals in the grid cell (Table 1, Fig. 3). We found highly localized areas of elevated average FOI on the landscape (Fig. 3). Notably, these hotspots were substantially smaller than individual home ranges (Fig. 3), where an average of only 13% of the area of an individual's home range (calculated as a 95% utilization distribution; Calenge 2006) contained 80% of potential FOI experienced by an individual. This builds on our results above, showing that fine-scale spatial heterogeneity in potential transmission risk exists on the landscape and can significantly affect spatial disease dynamics.

Discussion

There is a burgeoning recognition that our ability to quantify individual, spatial, and temporal heterogeneity in transmission risk would benefit from a tighter link between movement and disease ecology (Dougherty *et al.* 2018; Manlove *et al.* 2021). Here, we developed a framework that we call "Movement-driven modeling of spatio-temporal infection risk" (MoveSTIR). MoveSTIR provides a flexible framework to address key empirical and theoretical challenges in disease ecology. As we demonstrate with our simulations and empirical examples, MoveSTIR allows us to build direct and indirect contact networks across a continuum, derive spatially explicit metrics of transmission risk that can be easily integrated with landscape variables, and decompose the temporal dynamics of potential or realized infection hazard. MoveSTIR does this by linking epidemiological theory with commonly observed movement data. Importantly, application of MoveSTIR to real-life movement data demonstrated the significance of accounting for fine-scale individual movements.

We observed notably higher potential for pathogen invasion in a wild pig system when we used MoveSTIR to extract the detailed information on transmission-relevant contacts contained in our observed movement trajectories, compared to earlier approaches that ignore fine-scale host movements. Given the increasing availability of movement data across thousands of animal taxa (Kranstauber *et al.* 2011; Miller *et al.* 2019), MoveSTIR provides a flexible, generalizable framework that exploits the full potential of these data to understand the mechanistic underpinnings of individual, spatial, and temporal variation in transmission risk and improve epidemiological prediction.

The flexibility of MoveSTIR stems in part from its link to dynamic, epidemiological networks (Holme & Saramäki 2012; Enright & Kao 2018), a framework that MoveSTIR extends by quantifying the contributions of direct and indirect contact to network structure in an epidemiologically consistent way. Therefore, MoveSTIR generalizes much of the previous work on dynamic, static, weighted, directional or multi-layer contact networks derived from empirical contact and co-occurrence data. MoveSTIR also builds upon notable previous work with movement data, encounter rates, and epidemiological dynamics (Stehlé *et al.* 2011b; Gurarie & Ovaskainen 2013; Richardson & Gorochowski 2015; Martinez-Garcia *et al.* 2020; Zhang *et al.* 2020; Noonan *et al.* 2021). What distinguishes MoveSTIR from this previous work is that it is derived from epidemiological first principles and explicitly considers contact formation, contact duration, the continuum between direct to indirect contact, pathogen deposition, pathogen acquisition, how these rates might be modified by behavior, and the explicit units associated with each of these processes. Thus, MoveSTIR naturally confronts constituent processes of transmission that are usually shunted into the black box of β (McCallum *et al.* 2017) and can be expanded to account for additional complexities of transmission such as non-linear dose-response curves (Handel & Rohani 2015; Lunn *et al.* 2019).

While our application of MoveSTIR focused on wildlife, our framework is equally applicable to addressing questions regarding the spatio-temporal infection risk in humans and livestock. In humans, previous studies have used radio-frequency identification devices and mobile phone data to build contact networks and simulate epidemics (Stehlé *et al.* 2011a; Wesolowski *et al.* 2016; Panigutti *et al.* 2017). Similarly, livestock studies use proximity loggers to detect close proximity contacts (Lavelle *et al.* 2016; Kour *et al.* 2021). As described in Appendix S2, any of the MoveSTIR analyses we describe here can be applied to proximity data or array-like data (e.g., from mobile phone towers), whether or not these data are spatially explicit. Moreover, because MoveSTIR explicitly considers individual-level deposition and acquisition of a pathogen, information on how body position affects relative transmission risk (e.g., a face-to-face contact is more likely to lead to a transmission event than a back-to-face contact; Zhang *et al.* 2020; Kour *et al.* 2021) can be incorporated into MoveSTIR by allowing relative deposition and acquisition rates to depend on host behaviors (Appendix S1.2). Critically, application of MoveSTIR to wildlife, livestock, and human systems does

not necessarily require simultaneous infection data, as movement data and *a priori* assumptions on how particular behaviors and environments change relative deposition, acquisition, and pathogen decay rates are sufficient to make prospective inference on the spatio-temporal distribution of potential infection risk.

Despite its advantages, MoveSTIR has a few notable limitations. First, MoveSTIR infers contact networks and transmission risk from individuals whose movement trajectories have been observed at least partially. However, it is well-known that incomplete sampling of a network can affect epidemiological predictions and MoveSTIR does not resolve this issue (Silk *et al.* 2017). Second, MoveSTIR makes inference on spatio-temporal infection risk from one empirical realization of individual movement trajectories, potentially limiting the transportability of MoveSTIR predictions into new spatial and social contexts. Both of these limitation are not unique to MoveSTIR and are faced by most studies of empirical contact networks. However, MoveSTIR does provide exciting potential to address these challenges. If mechanistic movement models that depend on spatial and social context are used to fit the observed movement data (Hooten *et al.* 2017), then repeated simulation of movement trajectories predicted by these models could generate a distribution of spatio-temporal contacts networks in novel spatial and social environments and a corresponding distribution of epidemiological outcomes predicted by MoveSTIR. Thus, ongoing work in movement ecology to augment the out-of-sample prediction of host movements (e.g., Avgar *et al.* 2016) could directly improve the transportability of MoveSTIR's epidemiological predictions.

Overall, MoveSTIR is generalizable across host-pathogen systems, has clear epidemiological interpretation in spatial and temporal dimensions, is applicable to movement data that already exist for thousands of taxa and are increasingly being collected (Kranstauber *et al.* 2011), and provides a unifying epidemiological framework for how host movement data informs the individual, spatial, and temporal contributions to disease dynamics. Ultimately, MoveSTIR represents a key step toward improving the transportability of epidemiological predictions across spatial, temporal, and ecological contexts.

Acknowledgments

MW acknowledges the USDA National Institute of Food and Agriculture for funding (Hatch Project 1012932). RKB thanks the Archbold Buck Island Ranch for allowing the capture and study of wild pigs, as well as funding support from USDA APHIS Wild Pig Management Programs to conduct the work. Thanks to Nina Fefferman for useful discussions.

References

Aiello, C. M., Nussear, K. E., Esque, T. C., Emblidge, P. G., Sah, P., Bansal, S. & Hudson, P. J. (2016). Host contact and shedding patterns clarify variation in pathogen exposure and transmission in threatened tortoise *Gopherus agassizii*: Implications for disease modelling and management. *Journal of Animal Ecology*, 85, 829–842.

Albery, G. F., Kirkpatrick, L., Firth, J. A. & Bansal, S. (2020a). Unifying spatial and social network analysis in disease ecology. *Journal of Animal Ecology*, 1–17.

Albery, G. F., Sweeny, A. R., Becker, D. J. & Bansal, S. (2020b). Fine-scale spatial patterns of wildlife disease are common and understudied. *bioRxiv*, 2020.09.01.277442. URL `https://doi.org/10.1101/2020.09.01.277442`.

Arino, J. & van den Driessche, P. (2006). Time Delay in Epidemic Models. In: *Delay Differential Equations and Applications*. Springer, pp. 119–128.

Avgar, T., Potts, J. R., Lewis, M. A. & Boyce, M. S. (2016). Integrated step selection analysis: bridging the gap between resource selection and animal movement. *Methods in Ecology and Evolution*, 7, 619–630.

Bansal, S., Grenfell, B. T. & Meyers, L. A. (2007). When individual behaviour matters: homogeneous and network models in epidemiology. *Journal of The Royal Society Interface*, 4, 879–891.

Begon, M., Bennett, M., Bowers, R. G., French, N. P., Hazel, S. M. & Turner, J. (2002). A clarification of transmission terms in host-microparasite models: numbers, densities and areas. *Epidemiology and Infection*, 129, 147–153.

Burton, A. C., Neilson, E., Moreira, D., Ladle, A., Steenweg, R., Fisher, J. T., Bayne, E. & Boutin, S. (2015). Wildlife camera trapping: a review and recommendations for linking surveys to ecological processes. *Journal of Applied Ecology*, 52, 675–685.

Calabrese, J. M., Fleming, C. H. & Gurarie, E. (2016). CTMM: an R Package for analyzing animal relocation data as a continuous-time stochastic process. *Methods in Ecology and Evolution*, 7, 1124–1132.

Calenge, C. (2006). The package adehabitat for the R software: tool for the analysis of space and habitat use by animals. *Ecological Modelling*, 197, 1035.

Cayuela, H., Pradel, R., Joly, P. & Besnard, A. (2017). Analysing movement behaviour and dynamic space-use strategies among habitats using multi-event capture-recapture modelling. *Methods in Ecology and Evolution*, 8, 1124–1132.

Craft, M. E. (2015). Infectious disease transmission and contact networks in wildlife and livestock. *Philosophical Transactions of the Royal Society B: Biological Sciences*, 370, 20140107.

Cross, P. C., Johnson, P. L., Lloyd-Smith, J. O. & Getz, W. M. (2007). Utility of R0 as a predictor of disease invasion in structured populations. *Journal of the Royal Society Interface*, 4, 315–324.

Diekmann, O., Heesterbeek, J. A. P. & Britton, T. (2013). *Mathematical Tools for Understanding Infectious Disease Dynamics*. Princeton University Press, Princeton.

Dougherty, E. R., Seidel, D. P., Carlson, C. J., Spiegel, O. & Getz, W. M. (2018). Going through the motions: Incorporating movement analyses into disease research. *Ecology Letters*, 588–604.

Dwyer, G., Elkinton, J. S. & Buonaccorsi, J. P. (1997). Host heterogeneity in susceptibility and disease dynamics: tests of a mathematical model. *The American Naturalist*, 150, 685–707.

Enright, J. & Kao, R. R. (2018). Epidemics on dynamic networks. *Epidemics*, 24, 88–97.

Fefferman, N. H. & Ng, K. L. (2007). How disease models in static networks can fail to approximate disease in dynamic networks. *Physical Review E - Statistical, Nonlinear, and Soft Matter Physics*, 76, 1–11.

Fenton, A., Streicker, D. G., Petchey, O. L. & Pedersen, A. B. (2015). Are all hosts created equal? Partitioning host species contributions to parasite persistence in multihost communities. *The American Naturalist*, 186, 610–622.

Godfrey, S. S., Moore, J. A., Nelson, N. J. & Bull, C. M. (2010). Social network structure and parasite infection patterns in a territorial reptile, the tuatara (*Sphenodon punctatus*). *International Journal for Parasitology*, 40, 1575–1585.

Gurarie, E. & Ovaskainen, O. (2013). Towards a general formalization of encounter rates in ecology. *Theoretical Ecology*, 6, 189–202.

Handel, A. & Rohani, P. (2015). Crossing the scale from within-host infection dynamics to between-host transmission fitness: a discussion of current assumptions and knowledge. *Philosophical Transactions of the Royal Society B: Biological Sciences*, 370, 20140302.

Holme, P. & Liljeros, F. (2014). Birth and death of links control disease spreading in empirical contact networks. *Scientific Reports*, 4, 19–21.

Holme, P. & Saramäki, J. (2012). Temporal networks. *Physics Reports*, 519, 97–125.

Hooten, M. B., Johnson, D. S., McClintock, B. T. & Morales, J. M. (2017). *Animal Movement: Statistical Models for Telemtry data*. CRC Press, New York, USA.

Hooten, M. B., Scharf, H. R., Hefley, T. J., Pearse, A. T. & Weegman, M. D. (2018). Animal movement models for migratory individuals and groups. *Methods in Ecology and Evolution*, 2018, 1–14.

Hopkins, S. R., Fleming-Davies, A. E., Belden, L. K. & Wojdak, J. M. (2020). Systematic review of modelling assumptions and empirical evidence: Does parasite transmission increase nonlinearly with host density? *Methods in Ecology and Evolution*, 11, 476–486.

Jacoby, D. M. & Freeman, R. (2016). Emerging network-based tools in movement ecology. *Trends in Ecology and Evolution*, 31, 301–314.

Johnson, D. S., London, J. M., Lea, M.-A. & Durban, J. W. (2008). Continuous-Time Correlated Random Walk Model for Animal Telemetry Data. *Ecology*, 89, 1208–1215.

Kour, H., Patison, K. P., Corbet, N. J. & Swain, D. L. (2021). Recording cattle maternal behaviour using proximity loggers and tri-axial accelerometers. *Applied Animal Behaviour Science*, 240, 105349.

Kranstauber, B., Cameron, A., Weinzierl, R., Fountain, T., Tilak, S., Wikelski, M. & Kays, R. (2011). The Movebank data model for animal tracking. *Environmental Modelling and Software*, 26, 834–835.

Lavelle, M. J., Kay, S. L., Pepin, K. M., Grear, D. A., Campa, H. & VerCauteren, K. C. (2016). Evaluating wildlife-cattle contact rates to improve the understanding of dynamics of bovine tuberculosis transmission in Michigan, USA. *Preventive Veterinary Medicine*, 135, 28–36.

Leitch, J., Alexander, K. A. & Sengupta, S. (2019). Toward epidemic thresholds on temporal networks: a review and open questions. *Applied Network Science*, 4.

Lunn, T. J., Restif, O., Peel, A. J., Munster, V. J., De Wit, E., Sokolow, S., Van Doremalen, N., Hudson, P. & McCallum, H. (2019). Dose-response and transmission: the nexus between reservoir hosts, nvironment and recipient hosts. *Philosophical Transactions of the Royal Society B: Biological Sciences*, 374.

Manlove, K., Aiello, C., Sah, P., Cummins, B., Hudson, P. J. & Cross, P. C. (2018). The ecology of movement and behaviour: A saturated tripartite network for describing animal contacts. *Proceedings of the Royal Society B: Biological Sciences*, 285.

Manlove, K., Wilber, M., White, L., Bastille-Rousseau, G., Yang, A., Gilbertson, M. L. J., Craft, M., Cross, P., Wittemyer, G. & Pepin, K. (2021). Predicting epidemiological dynamics on real landscapes needs movement ecology. *In review*.

529 Martinez-Garcia, R., Fleming, C. H., Seppelt, R., Fagan, W. F. & Calabrese, J. M. (2020). How range
530 residency and long-range perception change encounter rates. *Journal of Theoretical Biology*, 498, 110267.

531 Mazur-Panasiuk, N., Żmudzki, J. & Woźniakowski, G. (2019). African swine fever virus - persistence in
532 different environmental conditions and the possibility of its indirect transmission. *Journal of Veterinary*
533 *Research (Poland)*, 63, 303–310.

534 McCallum, H., Barlow, N. & Hone, J. (2001). How should pathogen transmission be modelled? *Trends in*
535 *ecology and evolution*, 16, 295–300.

536 McCallum, H., Fenton, A., Hudson, P. J., Lee, B., Levick, B., Norman, R., Perkins, S. E., Viney, M., Wilson,
537 A. J. & Lello, J. (2017). Breaking beta: deconstructing the parasite transmission function. *Philosophical*
538 *Transactions of the Royal Society B*, 372, 20160084.

539 Meekan, M. G., Duarte, C. M., Fernández-Gracia, J., Thums, M., Sequeira, A. M., Harcourt, R. & Eguíluz,
540 V. M. (2017). The ecology of human mobility. *Trends in Ecology and Evolution*, 32, 198–210.

541 Miller, H. J., Dodge, S., Miller, J. & Bohrer, G. (2019). Towards an integrated science of movement:
542 converging research on animal movement ecology and human mobility science. *International Journal of*
543 *Geographical Information Science*, 33, 855–876.

544 Noonan, M. J., Martinez-Garcia, R., Davis, G. H., Crofoot, M. C., Kays, R., Hirsch, B. T., Caillaud, D.,
545 Payne, E., Sih, A., Sinn, D. L., Spiegel, O., Fagan, W. F., Fleming, C. H. & Calabrese, J. M. (2021).
546 Estimating encounter location distributions from animal tracking data. *Methods in Ecology and Evolution*,
547 2021, 1–16.

548 Panigutti, C., Tizzoni, M., Bajardi, P., Smoreda, Z. & Colizza, V. (2017). Assessing the use of mobile phone
549 data to describe recurrent mobility patterns in spatial epidemic models. *Royal Society Open Science*, 4,
550 160950.

551 Parratt, S. R., Numminen, E. & Laine, A.-l. (2016). Infectious disease dynamics in heterogeneous landscapes.
552 *Annual Review of Ecology, Evolution, and Systematics*, 47, 283–306.

553 Paull, S. H., Song, S., McClure, K. M., Sackett, L. C., Kilpatrick, A. M. & Johnson, P. T. J. (2012). From
554 superspreaders to disease hotspots: linking transmission across hosts and space. *Frontiers in ecology and*
555 *the environment*, 10, 75–82.

556 Richardson, T. O. & Gorochowski, T. E. (2015). Beyond contact-based transmission networks: the role of
557 spatial coincidence. *Journal of the Royal Society Interface*, 12.

Royle, J. A., Chandler, R. B., Sollmann, R. & Gardner, B. (2014). *Spatial Capture-Recapture*. Elsevier, Oxford.

Shahzamal, M., Jurdak, R., Mans, B. & De Hoog, F. (2019). Indirect interactions influence contact network structure and diffusion dynamics. *Royal Society Open Science*, 6, 190845.

Silk, M. J., Croft, D. P., Delahay, R. J., Hodgson, D. J., Weber, N., Boots, M. & McDonald, R. A. (2017). The application of statistical network models in disease research. *Methods in Ecology and Evolution*, 8, 1026–1041.

Silk, M. J., Drewe, J. A., Delahay, R. J., Weber, N., Steward, L. C., Wilson-Aggarwal, J., Boots, M., Hodgson, D. J., Croft, D. P. & McDonald, R. A. (2018). Quantifying direct and indirect contacts for the potential transmission of infection between species using a multilayer contact network. *Behaviour*, 155, 731–757.

Silk, M. J., Hodgson, D. J., Rozins, C., Croft, D. P., Delahay, R. J., Boots, M., Mcdonald, R. A., Silk, M. J. & Mcdonald, R. A. (2019). Integrating social behaviour, demography and disease dynamics in network models: applications to disease management in declining wildlife populations. *Philosophical Transactions of the Royal Society B*, 374, 20180211.

Silk, M. J., McDonald, R. A., Delahay, R. J., Padfield, D. & Hodgson, D. J. (2021). CMRnet: An r package to derive networks of social interactions and movement from mark–recapture data. *Methods in Ecology and Evolution*, 12, 70–75.

Springer, A., Kappeler, P. M. & Nunn, C. L. (2017). Dynamic vs. static social networks in models of parasite transmission: predicting *Cryptosporidium* spread in wild lemurs. *Journal of Animal Ecology*, 86, 419–433.

Stehlé, J., Voirin, N., Barrat, A., Cattuto, C., Colizza, V., Isella, L., Régis, C., Pinton, J.-f., Khanafer, N., Broeck, V. D. & Vanhems, P. (2011a). Simulation of a SEIR infectious disease model on the dynamic contact network of conference attendees. *BMC Medicine*, 9, 1–4.

Stehlé, J., Voirin, N., Barrat, A., Cattuto, C., Isella, L., Pinton, J. F., Quaggiotto, M., van den Broeck, W., Régis, C., Lina, B. & Vanhems, P. (2011b). High-resolution measurements of face-to-face contact patterns in a primary school. *PLoS ONE*, 6, e23176.

Valdano, E., Ferreri, L., Poletto, C. & Colizza, V. (2015). Analytical computation of the epidemic threshold on temporal networks. *Physical Review X*, 5, 1–9.

VanderWaal, K., Enns, E. A., Picasso, C., Packer, C. & Craft, M. E. (2016). Evaluating empirical contact networks as potential transmission pathways for infectious diseases. *Journal of The Royal Society Interface*, 13, 20160166.

Virtanen, P., Gommers, R., Oliphant, T. E., Haberland, M., Reddy, T., Cournapeau, D., Burovski, E., Peterson, P., Weckesser, W., Bright, J., van der Walt, S. J., Brett, M., Wilson, J., Millman, K. J., Mayorov, N., Nelson, A. R. J., Jones, E., Kern, R., Larson, E., Carey, C. J., Polat, İ., Feng, Y., Moore, E. W., VanderPlas, J., Laxalde, D., Perktold, J., Cimrman, R., Henriksen, I., Quintero, E. A., Harris, C. R., Archibald, A. M., Ribeiro, A. H., Pedregosa, F., van Mulbregt, P. & SciPy 1.0 Contributors (2020). SciPy 1.0: fundamental algorithms for scientific computing in Python. *Nature Methods*, 17, 261–272.

Wesolowski, A., Buckee, C. O., Engø-Monsen, K. & Metcalf, C. J. (2016). Connecting mobility to infectious diseases: the promise and limits of mobile phone data. *Journal of Infectious Diseases*, 214, S414–S420.

White, L. A., Forester, J. D. & Craft, M. E. (2017). Using contact networks to explore mechanisms of parasite transmission in wildlife. *Biological Reviews*, 92, 389–409.

Wilber, M. Q., Pepin, K. M., Campa Iii, H., Hygnstrom, S. E., Lavelle, M. J., Xifara, T., Vercauteren, K. C. & Webb, C. T. (2019). Modeling multi-species and multi-mode contact networks: implications for persistence of bovine tuberculosis at the wildlife-livestock interface. *Journal of Applied Ecology*, 56, 1471–1481.

Yang, A., Boughton, R. K., Miller, R. S., Wight, B., Anderson, W. M., Beasley, J. C., Vercauteren, K. C., Pepin, K. M. & Wittemyer, G. (2021). Spatial variation in direct and indirect contact rates at the wildlife-livestock interface for informing disease management. *Preventive Veterinary Medicine*, 194, 105423.

Yang, A., Schlichting, P., Wight, B., Anderson, W. M., Chinn, S. M., Wilber, M. Q., Miller, R. S., Beasley, J. C., Boughton, R. K., Vercauteren, K. C., Wittemyer, G., Pepin, K. M. & Yang, A. (2020). Effects of social structure and management on risk of disease establishment in wild pigs. *Journal of Animal Ecology*, 1–14.

Zhang, N., Su, B., Chan, P. T., Miao, T., Wang, P. & Li, Y. (2020). Infection spread and high-resolution detection of close contact behaviors. *International Journal of Environmental Research and Public Health*, 17.

Table 1: Compendium of integrals of $K_{a_i \leftarrow d_j}(\tau_a, \tau_d)$ to understand pairwise, spatio-temporal patterns in infection risk. We also provide a visualization of the mathematical formula as a matrix operation when the transmission kernel is represented with a grid approximation. The shaded entries indicate which grid cells are "summed" in correspondence with the integral (Appendix S1).

Definition	Mathematical formula	Units	Matrix operation
$h_{i \leftarrow j}(t)$: Force of infection (FOI) experienced by host i from host j at time t	$\int_0^t K_{a_i \leftarrow d_j}(t, u)du$	time^{-1}	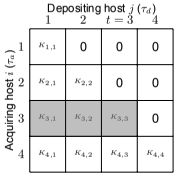
$H_{i \leftarrow j}(t)$: The cumulative FOI experienced by host i from host j from time $t = 0$ to time t	$\int_0^t \int_0^\tau K_{a_i \leftarrow d_j}(\tau, u)du d\tau$	unitless	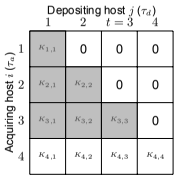
$\bar{h}_{i \leftarrow j}(t)$: The average FOI experienced by host i from host j from time $t = 0$ to time t	$\frac{H_{i \leftarrow j}(t)}{t}$	time^{-1}	Same as above divided by t
$\tilde{h}_{i \leftarrow j}(t)$: Force of infection contributed by host j at time t to host i's cumulative FOI	$\int_t^{t_{\text{end}}} K_{a_i \leftarrow d_j}(u, t)du$	time^{-1}	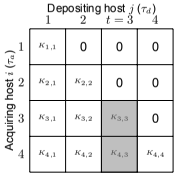
$\pi_{i \leftarrow j}(\Delta t, c, t)$: Proportional contribution from past and present host j from time $[\Delta t,\ \Delta t + c]$ to host i's cumulative FOI at time t, where Δt is the lag time from the current time t. This function computes the relative contributions of direct and indirect transmission to infection risk. $\delta_{\tau-u}(\rho)$ is a Dirac delta function.	$\frac{\int_{\rho=\Delta t}^{\Delta t+c} \int_{\tau=0}^{t} \int_{u=0}^{\tau} K_{a_i \leftarrow d_j}(\tau, u)\delta_{\tau-u}(\rho)du d\tau d\rho}{H_{i \leftarrow j}(t)}$	unitless	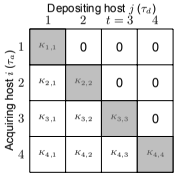 / $H_{i \leftarrow j}(4)$
$\bar{h}^A_{i \leftarrow j}(t)$: Average FOI experienced by host i from host j in spatial area A up to time t. The function $\mathbb{1}_{s_i(u)}$ is one if the location of host i at time u given by $s_i(u)$ is in area A and zero otherwise.	$\frac{\int_0^t h_{i \leftarrow j}(u)\mathbb{1}_{s_i(u) \in A}du}{\int_0^t \mathbb{1}_{s_i(u) \in A}du}$	time^{-1}	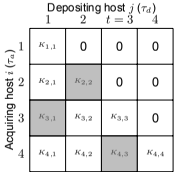 / Time in area A

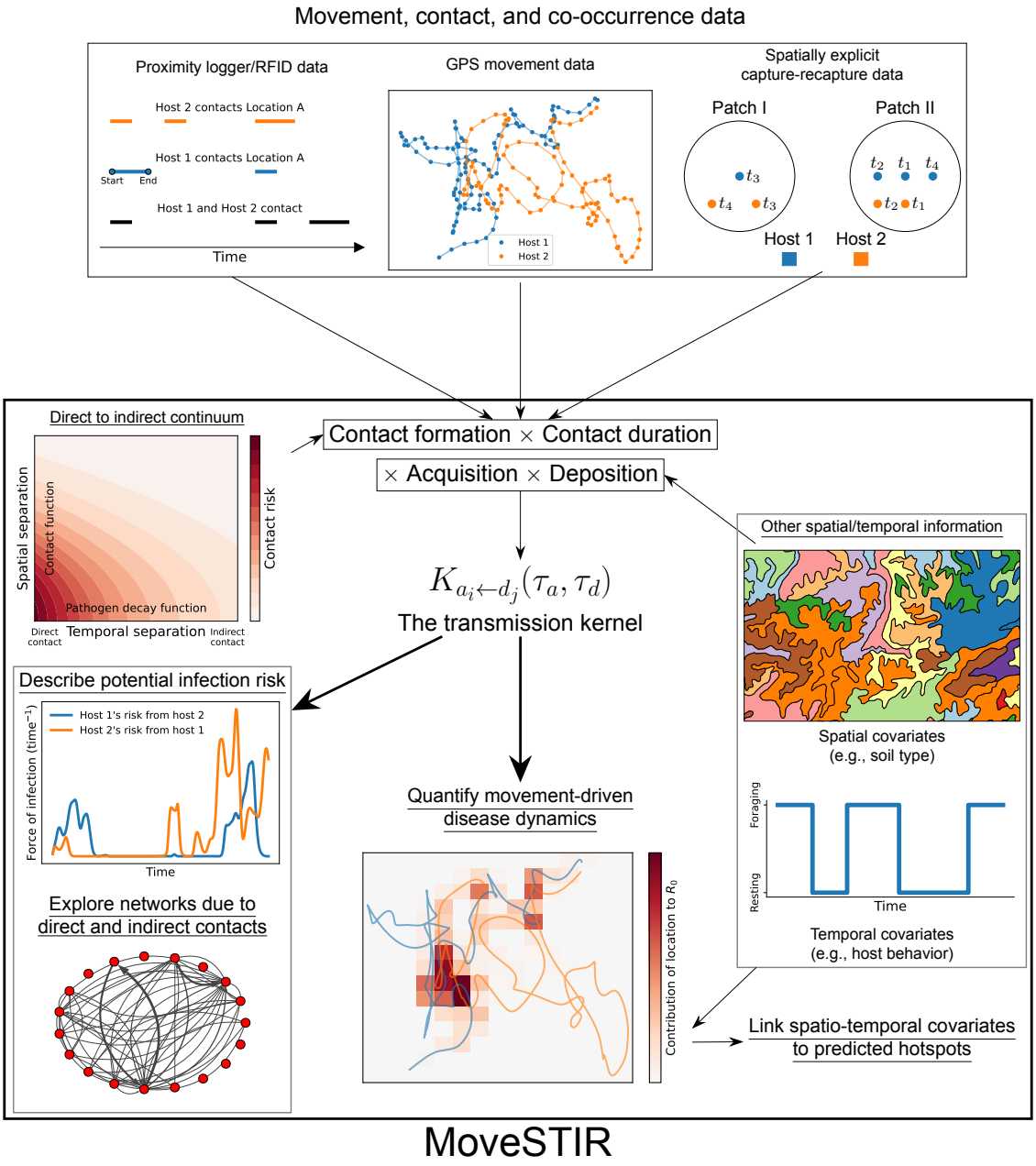

Figure 1: A conceptual overview of movement-driven modeling of spatio-temporal infection risk (MoveSTIR). The inputs to MoveSTIR are movement, contact, and co-occurrence data, which could take on a wide variety of forms (top panel). These data, with the help of continuous-time movement models, allow us to construct "contact" networks along a continuum of contact definitions. These networks, along with epidemiological information on pathogen decay, deposition, and acquisition, define the backbone of MoveSTIR – the transmission kernel. The transmission kernel can capture epidemiological assumptions (e.g., pathogen decay), describe potential infection risk among hosts, explore the structure of static or temporal contact and transmission networks, and be used to explore movement-driven disease dynamics on real landscapes.

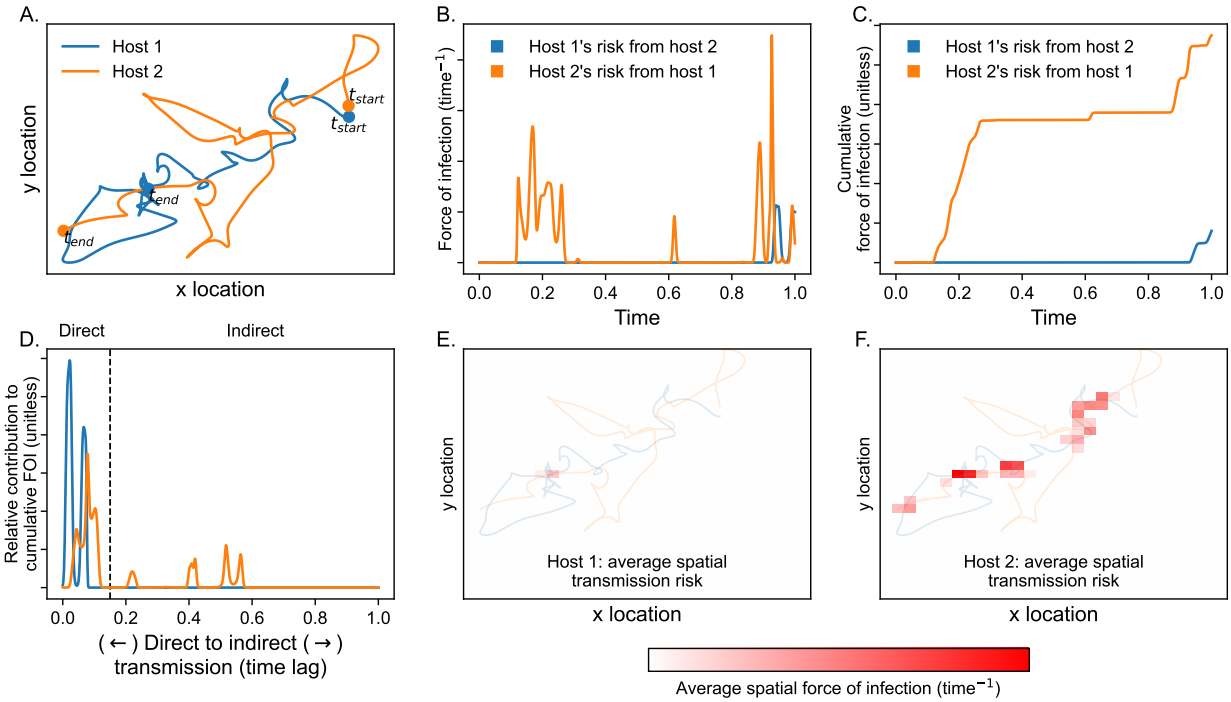

Figure 2: **A.** Simulated movement trajectories of two hosts through continuous space and time. The points t_{start} indicate the time when the movement trajectories start and t_{end} indicate when they end. **B.** The maximum potential force of infection (FOI) experienced by host 1 from host 2's movements and vice-versa as calculated from the transmission kernel (Table 1). **C.** Similar to B., but the potential cumulative FOI experienced by host 1 from host 2's movement (and vice-versa) at any time t (Table 1). **D.** The relative contribution of direct (time lag equal 0) to increasingly indirect (time lag > 0) transmission to the maximum cumulative FOI experienced by host 1 from host 2 (and vice-versa). The dashed line shows a pre-determined dichotomy between direct and indirect transmission. **E.** The average FOI experienced by host 1 from host 2 in a spatial area (given by grid cells on the plot) over the entire trajectory (see Table 1 for calculation). The colored lines show the host trajectories as shown in A. **F.** Same as E. but the average FOI experienced by host 2 from host 1 in a spatial area. For all figures, the transmission kernel is given by equation 5. We consider maximum potential infection risk by setting $\delta_{I_j(\tau_d)}(I) = 1$ for all j. The contact function $\Phi(\mathbf{s}_j(\tau_d), \mathbf{s}_i(\tau_a))$ follows a Gaussian function that depends on the Euclidean distance between locations $\mathbf{s}_j(\tau_d)$ and $\mathbf{s}_i(\tau_a)$, with a distance decay parameter $\alpha = 0.1$ (Appendix S1.1; Gurarie & Ovaskainen 2013). We assume that acquisition rate is $\tilde{\beta} = 1$ area / time, deposition rate is $\lambda = 1$ time^{-1}, pathogen decay is $\nu = 2$ time^{-1} such that a pathogen on average survives for half of a one unit time interval.

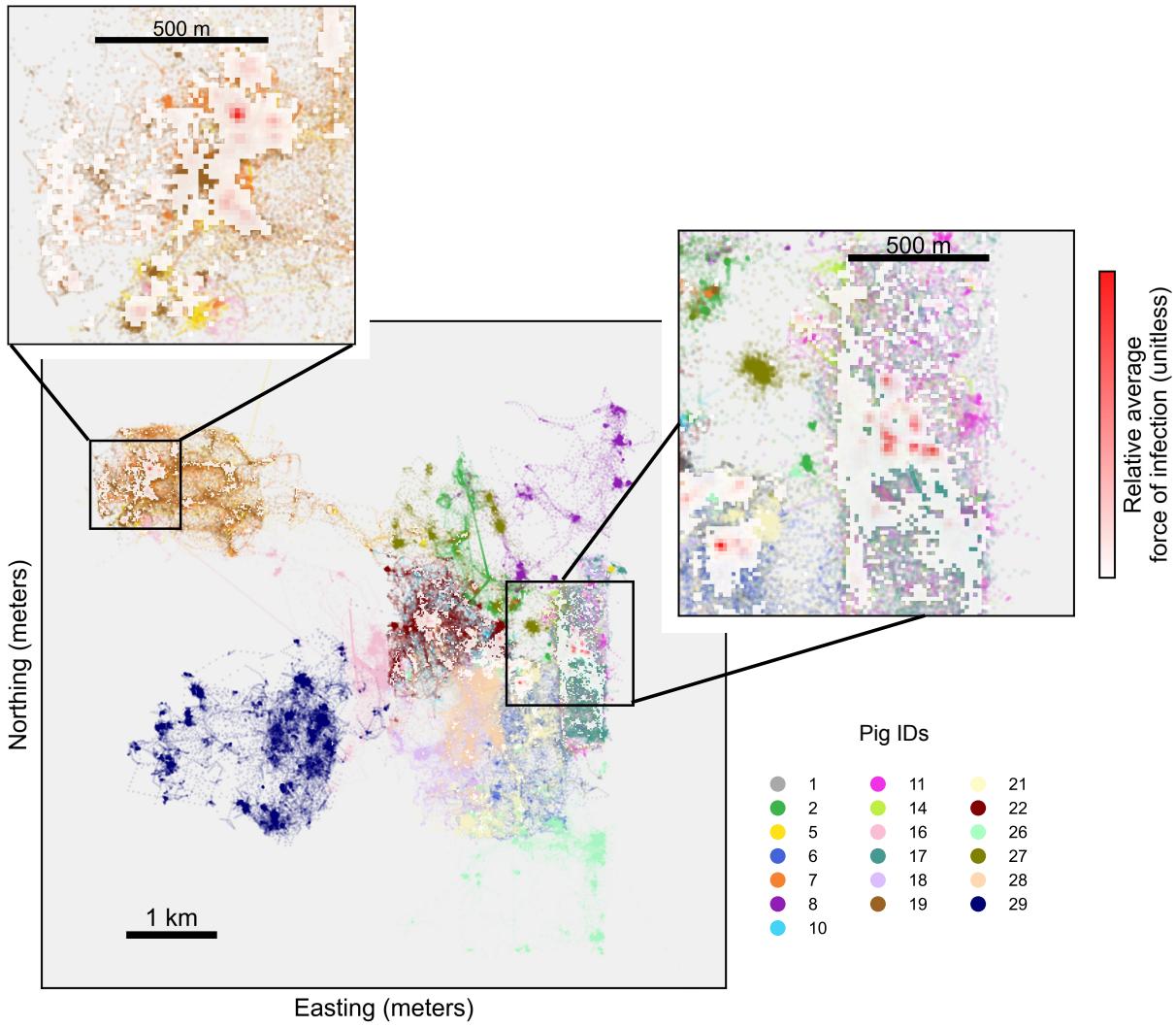

Figure 3: Map of observed pig movements on the landscape interpolated using continuous-time movement models at a scale of 5 minutes per time step (Calabrese *et al.* 2016) . Colored points show the movement trajectories for individual pigs. We overlaid 15 m by 15 m grids cells on the landscape and for each grid cell used MoveSTIR to calculate the relative average force of infection (FOI) across all individuals at a particular location. The color of grid cells range from transparent (minimal or no FOI experienced at the location) to dark red (high relative FOI experienced at the location). We calculated average FOI using $\bar{h}^{A}_{i \leftarrow j}(t)$ (Table 1), extending the metric to sum over all individuals that were ever in the spatial area A (i.e., a grid cell).

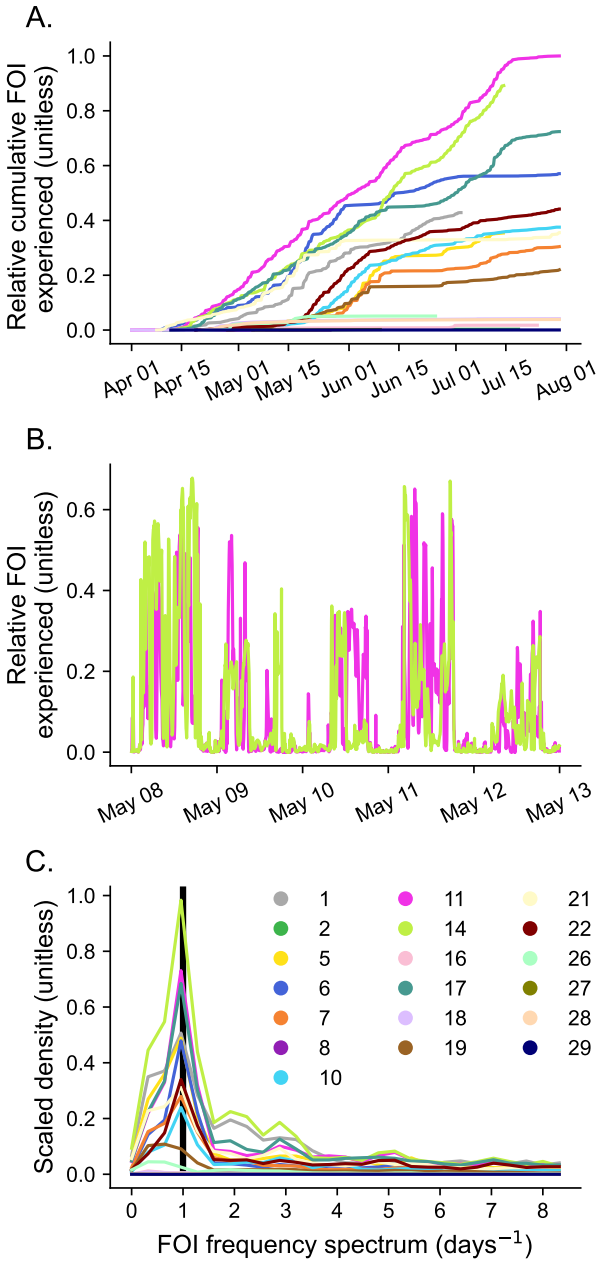

Figure 4: **A.** The relative potential cumulative force of infection (FOI) experienced by each individual pig through time from all other collared individuals ($\sum_{j \in S} H_{i \leftarrow j}(t)$ where S is the set of collared pigs, Table 1). All curves are standardized by the maximum cumulative FOI across all individuals. The derivatives of these curves give the temporal trajectories of FOI for each individual. Different colors refer to different individuals. **B.** The relative FOI experienced by individuals 11 and 14 over a five day interval ($\sum_{j \in S} h_{i \leftarrow j}(t)$, Table 1) within the four month study period. We only show individuals 11 and 14 for visual clarity. **C.** The power spectral density of temporal FOI (i.e., the trajectories in B. for all individuals over the four month study). We used the spectral density to identify patterns of periodicity in the time-series of FOI inferred by MoveSTIR (using Welch's method, Virtanen *et al.* 2020). The thick black vertical line indicates daily periodicity of FOI trajectories (period = 1 / frequency).

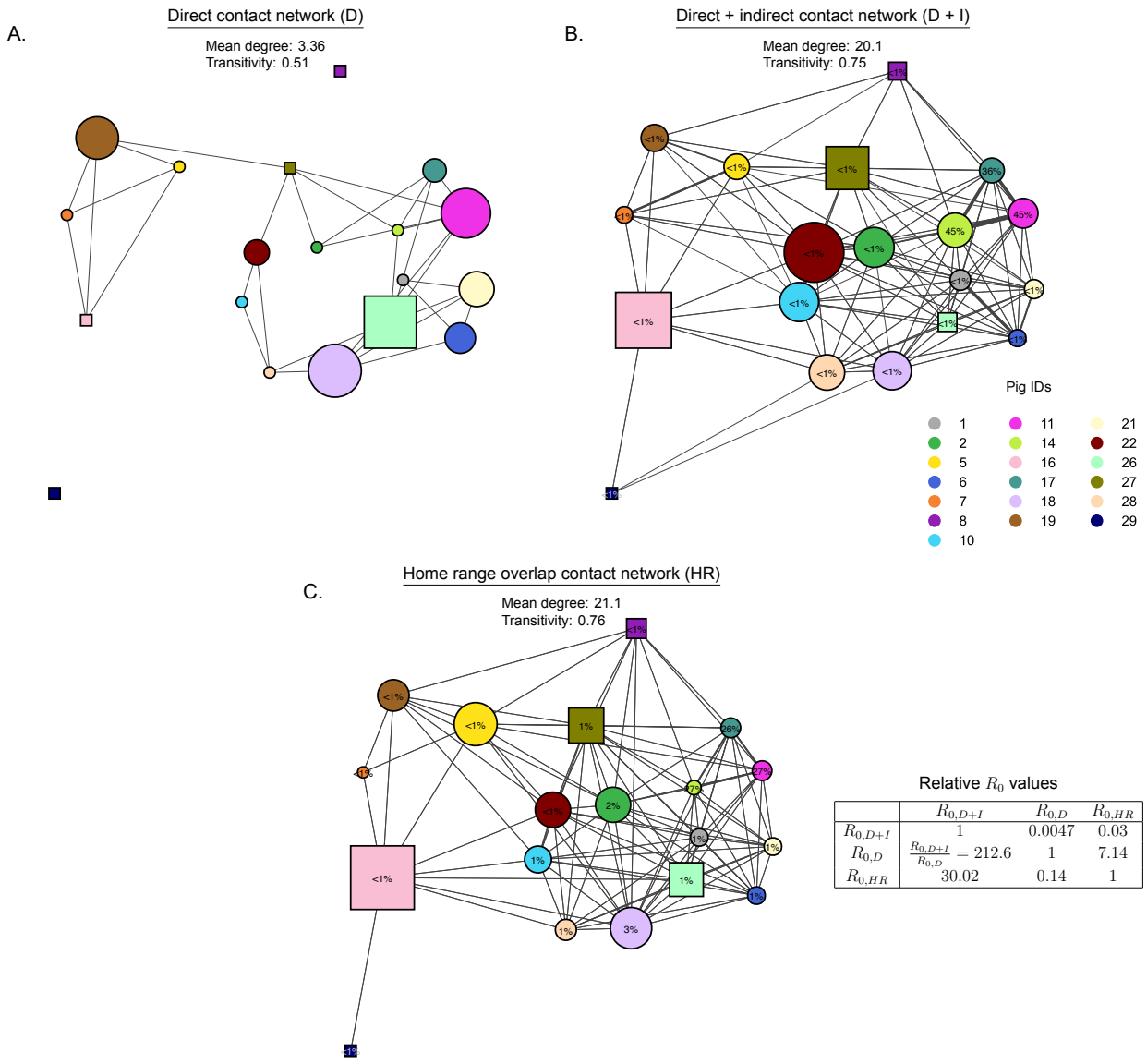

	$R_{0,D+I}$	$R_{0,D}$	$R_{0,HR}$
$R_{0,D+I}$	1	0.0047	0.03
$R_{0,D}$	$\frac{R_{0,D+I}}{R_{0,D}} = 212.6$	1	7.14
$R_{0,HR}$	30.02	0.14	1

Figure 5: **A.** The direct contact network inferred by MoveSTIR where direct contact is defined as hosts that are in the same place within a five-minute window. Direct contact is necessarily symmetric (at least in the limit as the temporal window size goes to zero), so the direct contact network is not a directed graph. Differential edge weights are not shown, but are defined as the average FOI due to direct transmission experienced between pairs of individuals over their collaring time ($\bar{h}_{i \leftarrow j}(t)$, Table 1). Edge weights were substantially less for direct contact compared to indirect contact making visual comparison difficult. **B.** The full contact network including both direct and indirect contacts. Different edge widths indicate scaled edge weights that give the average potential force of infection (FOI) between pairs of individuals over their collaring times. The full contact network is directed, but the directed arrows are not shown for clarity as many pairwise, directed interactions were relatively symmetrical. The numbers within the nodes give the percent that R_0 for the full network was reduced when a specific individual was removed. **C.** Similar to B., but the network was derived using the overlap of the 95% utilization distributions for the individual pigs (Appendix S6). For all networks, the size of the node gives a scaled measure of the betweenness centrality of the node (i.e., the frequency that a node resides on the shortest path between other nodes in the network). Betweenness values are scaled within a network. The mean degree and transitivity are calculated on the unweighted version of the network. Squares represent males and circles represent females. Finally, the table shows the relative R_0 values calculated by MoveSTIR for the networks in A.-C. (Appendix S4).